https://doi.org/10.5194/egusphere-2025-2512
Preprint. Discussion started: 10 June 2025

Petrophysics-guided reprocessing of legacy seismic data to improve mineral exploration targeting in the Irish Zn-Pb Orefield

Victoria Susin[1,2], Aline Melo[1,2], Koen Torremans[1,2], Juan Alcalde[3], David Martí[3], and Rafael Bartolome[4]

[1,2] School of Earth Sciences and Research Ireland Centre for Applied Geosciences (iCRAG), University College Dublin, Belfield, Dublin, Ireland
[3] Geosciences Barcelona GEO3BCN, Barcelona, Spain
[4] Instituto de Ciencias del Mar (ICM) CSIC, Barcelona, Spain

Correspondence to: Victoria Susin (victoria.figueirasusin@ucdconnect.ie)

Abstract. The Limerick Syncline, part of the Irish Zn-Pb Orefield in southwest Ireland, represents a geologically complex and relatively underexplored region, despite hosting several significant mineral deposits, e.g., Stonepark and Pallas Green. The mineralogy and stratigraphic setting of the sulphide mineralisation in the Limerick Syncline are generally similar to other Irish-type deposits. However, a thick volcanic sequence overlies and interfingers with the carbonate host rocks, mineralisation and alteration. This setting has posed significant challenges to seismic imaging in the region, despite being a powerful technique for mineral exploration. As a result, the overall structural setting of the area has remained poorly understood. This study presents an optimised seismic processing workflow tailored to these geological complexities and applied to the legacy 2D seismic reflection profile LK-11-02. The workflow integrates newly acquired downhole and laboratory P-wave velocity data with first-arrival travel-time tomography to enhance the accuracy of the velocity model used for post-stack migration. This resulted in better signal recovery and enhanced reflector coherence, in particular, reflection continuity. As a result, imaging of key stratigraphic boundaries and carbonate-volcanic interplay geometries was enhanced, along with clearer reflection amplitude changes associated with known stratigraphic units. Acoustic impedance analysis using laboratory density data enabled a better understanding of the origins of seismic reflectivity and a more confident geological interpretation of the laterally variable lithologies. The migrated section reveals previously unrecognised major structural features in the Limerick Syncline, enhancing our geological understanding of the region. It highlights the potential of applying this workflow to seismic reflection methods, improving its use as a mineral exploration tool in the Irish Zn-Pb Orefield and similar volcanic-influenced regions.

1 Introduction

The transition to a low-carbon society has significantly increased the demand for essential resources in recent years, driving higher consumption of base metals and critical materials needed for advancing sustainable technologies (Vidal et al., 2013; Ali et al., 2017). Meanwhile, the depth to target across the mining industry continues to increase globally (Alcalde et al., 2022). Specifically in Europe, the recent Critical Raw Materials Act (CRMA) has reinforced the need for sustainable sourcing of critical raw materials within the European Union (Hool et al., 2024), requiring increasingly comprehensive analysis of the subsurface resources. This incentivises the development of cost-effective, more sustainable and high-resolution geophysical methods for mineral exploration (Malehmir et al., 2020; Alcalde et al., 2022).

Due to the relatively limited resolving power of traditional mining geophysical methods – such as electromagnetics, induced polarisation, and potential field techniques – at greater depths, the adoption of methods from the oil and gas industry has gradually become more common in mineral exploration (Eaton et al., 2003). The seismic reflection method can provide high-resolution images of the subsurface with a greater penetration depth, complementing and defining target areas for drilling campaigns, which has led to the growing interest in seismic methods as a mineral exploration tool. Its relatively recent success in imaging and characterising mineral prospects and their structural controls, depth extensions, and host rock properties has

https://doi.org/10.5194/egusphere-2025-2512
Preprint. Discussion started: 10 June 2025

been highlighted in multiple studies (e.g., Eaton and Adam, 2010; Malehmir et al., 2012; Manzi et al., 2019; Malehmir et al., 2020; Gil et al., 2021; Cheraghi et al., 2023; Bell et al., 2023).

In Ireland, 2D seismic surveys have been conducted to better understand the structural and stratigraphic setting of the Irish Mississippian basins to assist exploration for Irish Type Zn-Pb deposits (e.g., de Morton et al., 2015; Ashton et al., 2018). These deposits are hosted within hydrothermally altered carbonate rocks and are predominantly associated with normal faults in relay-ramp systems (Wilkinson and Hitzman, 2015). Spanning an area of approximately 40,000 km^2, the Irish Orefield has been a significant focus of exploration. Since the 1950s, five deposits, including Lisheen, Galmoy and the world-class Navan deposit, have been developed into producing mines (Blaney and Redmond, 2015).

Ashton et al. (2018) reported the successful application of seismic reflection to the discovery of the Tara Deep deposit at depths of 1,500 meters, in the vicinity of the Navan deposit. Currently, around 1000 line-km of 2D reflection seismic exists across the Irish Midlands.

As part of mineral exploration efforts, six 2D seismic reflection profiles were acquired in 2011 near the Stonepark and Pallas Green Zn-Pb deposits, on the northwestern edge of the Limerick Syncline, the study area of this contribution, in southwest Ireland (Fig. 1). The Stonepark deposit has a resource of 5.1 Mt grading 8.7% Zn and 2.6% Pb at depths of 200 meters, and the Pallas Green deposit, a resource of 45.4 Mt grading 7% Zn and 1% Pb at depths between 200 and 1,000 meters (Gordon et al., 2018; Blaney and Coffey, 2023).

In this area, the carbonate rocks that host the sulphide mineralisation are intruded by and interbedded with a thick volcanic succession (Blaney and Coffey, 2023), whose distribution is still poorly understood. Volcanic rocks pose difficulties for seismic imaging because of signal attenuation (Liberty et al., 2015; McBride et al., 2021) and scattering, caused by abrupt vertical changes in elastic properties (e.g., Pujol et al., 1989; Planke et al., 1999; Ziolkowski et al., 2003; Sullivan et al., 2011). These effects have discouraged further seismic exploration in the target area due to the low resolution obtained in previous imaging efforts.

The effectiveness of seismic methods is highly site- and geology-dependent (Malehmir et al., 2012). In geologically complex settings like the Limerick Syncline, characterised by abrupt lateral facies changes (Somerville et al., 2011), effective seismic processing with suitable velocity models and migration algorithms is crucial to achieve a reliable seismic image (Singh and Malinowski, 2023). Additionally, lithological and petrophysical characteristics of the stratigraphic units, especially the volcanic rocks, must be considered during data processing to ensure accurate imaging and preserve true amplitude responses (Planke et al., 1999). However, suitable velocity models and well-constrained petrophysical data are currently missing for the Irish Midlands, especially for the Limerick Syncline. Furthermore, a robust interpretation of the acoustic impedance variations and the origin of seismic reflectivity remains absent in this part of the basin.

Therefore, to improve the imaging of the subsurface of the study area, we developed and implemented a reprocessing workflow on the legacy profile LK-11-02 to establish a benchmark for seismic data processing in the Irish Mississippian, applied to the Limerick Syncline area (Fig. 1). This new processing sequence incorporates recently acquired downhole and laboratory petrophysical data, along with first-arrival travel-time tomography, which provided essential insights into the velocity field, distinguishing it from previous seismic reflection workflows.

We also present an interpretation of the new velocity data, exploring the petrophysical characteristics of the main units in the Limerick Syncline and how the laboratory P-wave velocity correlates with the travel-time tomography. We used this information to build a new stacking velocity model, leading to an improved seismic image with enhanced resolution. Using

https://doi.org/10.5194/egusphere-2025-2512
Preprint. Discussion started: 10 June 2025

the resulting improved image, we provide an interpretation highlighting the main lithologic boundaries and fault zones, discussing the potential of seismic imaging in the subsurface characterisation and mineral exploration of the area.

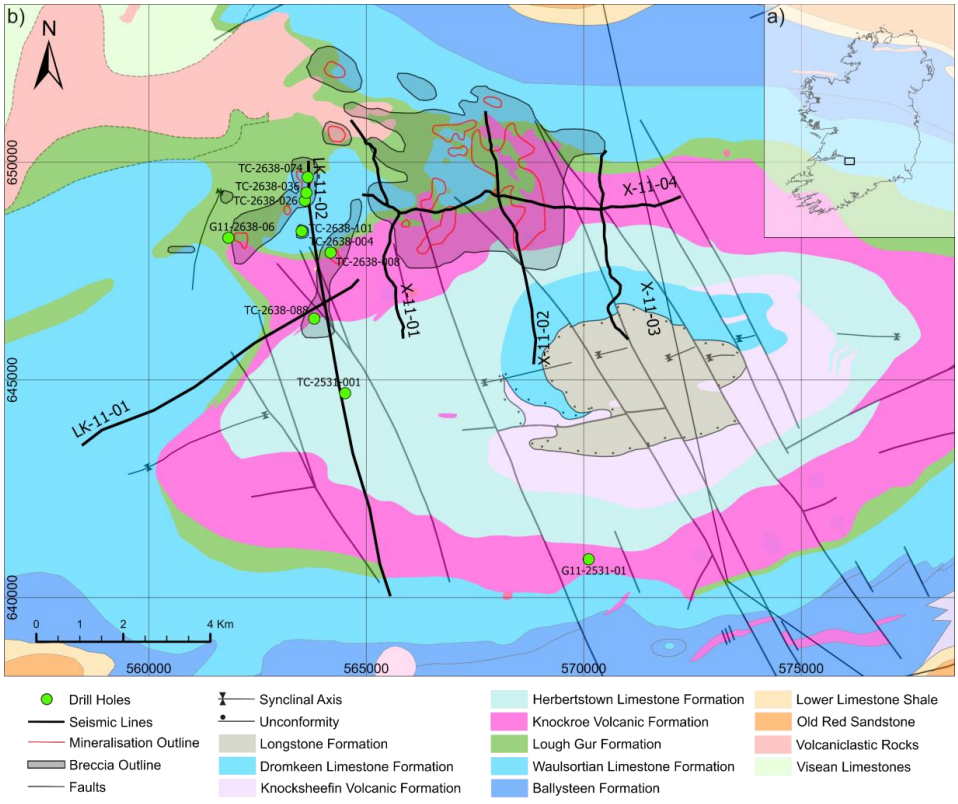

Figure 1: a) Map of Ireland with Limerick Syncline location (black rectangle). b) Geological map of the Limerick Syncline 1:100,000 (Geological Survey of Ireland, 2022) showing the drill holes used for downhole and laboratory petrophysical measurements (green circles) and the location of the Stonepark and Pallas Green prospects.

2 Geological setting

The Limerick Syncline hosts a stratigraphic sequence consisting of siliciclastic, carbonate and volcanic rocks (Somerville et al., 1992; Fig. 2). The Lower Palaeozoic basement, underlying the basinal succession, consists of greywackes, shales and volcanic rocks deformed and weakly metamorphosed during the Caledonian orogeny (Chew and Stillman, 2009). Lying unconformably atop the basement are largely Devonian continental red bed conglomerates, sandstones, and mudrocks of the Old Red Sandstone Formation, likely deposited in grabens. A northward-directed marine transgression across Ireland occurred during the early Mississippian, depositing progressively deeper marine carbonates (Sevastopulo and Wyse Jackson, 2009). The oldest transgressive unit is the Lower Limestone Shale Group (LLS), comprising a heterolithic series of interbedded shales, siltstones and sandstones, and carbonates (Somerville and Jones, 1985; Tyler, 1997; Blaney and Redmond, 2015). A transition to fully marine sedimentation followed in an open carbonate ramp environment, consisting of a sequence of argillaceous bioclastic limestones (ABL) of the Ballymartin Formation and Ballysteen Formation, together forming the Ballysteen Group. Finally, increasing water depths allowed the development of laterally extensive sequences of micritic mud mounds of the Waulsortian Limestone Formation (WAL; Somerville and Jones, 1985).

https://doi.org/10.5194/egusphere-2025-2512
Preprint. Discussion started: 10 June 2025

Above the WAL lies the Lough Gur Formation (LGG), a cherty, bioclastic, argillaceous limestone, succeeded by the Knockroe Volcanic Formation (KKR), a series of basaltic lavas and pyroclastic strata variably altered and brecciated (Strogen, 1988; Somerville et al., 1992; Blaney and Coffey, 2023). The KKR is interfingered with the carbonate beds of the LGG and the overlying Herbertstown Limestone Formation (HBN), dominated by grainstones and packstones of shallow water origin (Somerville et al., 1992). Towards the top, HBN is interbedded with the Knocksheefin Volcanic Formation (KKS), consisting of variably altered basanites and tuffs. Chlorite-clay alteration is typically seen in both KKR and KKS (Slezak et al., 2023). The interfingering of volcanics and carbonates forms a package up to 900 meters thick in the Limerick Syncline. These units are cut by later porphyritic basalt dykes and sills (Strogen, 1983; Slezak et al., 2023).

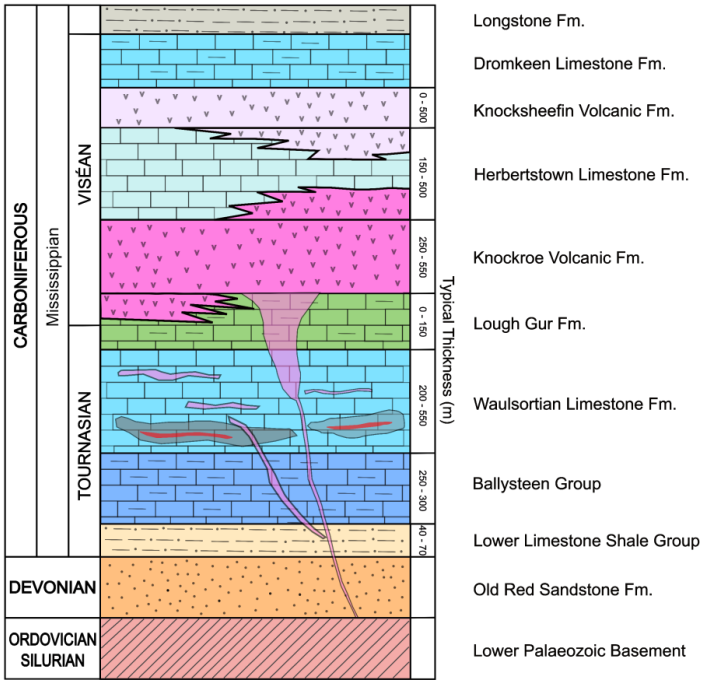

Figure 2: Stratigraphic column of Limerick Syncline (adapted from Somerville and Jones, 1985; Strogen, 1988; Somerville et al., 1992; Blaney and Redmond, 2015). Brecciated zones are drawn in grey and Zn-Pb mineralisation in red.

The Waulsortian-hosted Zn-Pb deposits occur largely in the hanging walls of complexly segmented relay-ramp normal fault systems (Hitzman, 1999; Torremans et al., 2018; Kyne et al., 2019). These fault zones are associated with Early Mississippian rifting in the Midlands, having a similar age to the upper ABL and WAL deposition (Johnston et al., 1996; de Morton et al., 2015). Previously, Somerville and Strogen (1992) have argued the absence of syn-sedimentary faulting in the Shannon Trough, and, to date, no large ore-controlling faults have been identified in the study area (Blaney and Redmond, 2015). Blaney and Coffey (2023) discuss the association between intrusions in the Limerick Syncline and syn-volcanic faults, and the possibility that these faults were the primary conduits for mineralising fluids. In the study area, most of the mineralisation occurs within the lower half of the WAL as stratiform lenses hosted by breccia bodies. Brecciation and mineralisation formed through alteration and precipitation-dissolution processes by hydrothermal fluids (Blaney and Redmond, 2015).

https://doi.org/10.5194/egusphere-2025-2512
Preprint. Discussion started: 10 June 2025

3 Data and Methods

This study focuses on the reprocessing of profile LK-11-02, which is part of a series of 2D surveys acquired on the northwestern edge of the Limerick Syncline (Fig. 1). Figure 3 illustrates the workflow employed in this study. The processing workflow incorporates new acquisition of on-core petrophysical data through laboratory measurements and the use of legacy sonic log data. This data was used to produce an iteratively refined velocity analysis, integrating P-wave velocity (Vp) from the laboratory and downhole petrophysics, travel-time tomography from legacy first-break picks, and semblance analysis from legacy CDP gathers. Two legacy seismic datasets were used as input for the new processing, which included an optimised velocity analysis and time migration. Additionally, acoustic impedance data were derived from the petrophysical properties to assist in a more comprehensive and geology-driven seismic interpretation.

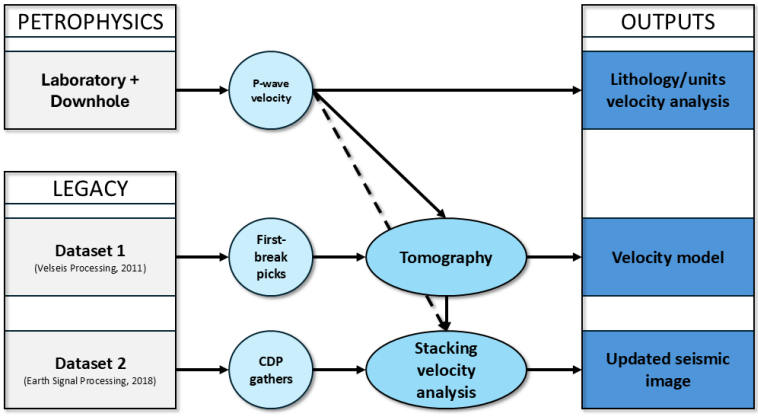

Figure 3: Flowchart showing the data and processing workflow used in the study. Legacy dataset 1 and legacy dataset 2 comprise the data made available for the new processing. Outputs are the workflow and products that we developed to improve the seismic image.

3.1 Drill hole data

Ten drill holes with associated geological logs were made available for this work. Drilled depths range from 350 to 900 meters (Table 1). Eight of these drill holes are located on or near the seismic profile trace, while the remaining two (G11-2531-01 and G11-2638-06) are situated 4.9 and 1.8 km away, respectively (Fig. 1). The drill holes predominantly intersect the WAL, typically finishing several meters into the underlying ABL. Only two of the eight drill holes along the seismic line sample the shallower stratigraphic units.

The top of drill hole TC-2638-088 (Fig. 1) intersects the KKR for 95 meters, followed by 70 meters of LGG before reaching the WAL and the top of the ABL. South of TC-2638-088, in the central part of the seismic profile, the drill hole TC-2531-001 is the deepest in the region, providing 926.60 meters of stratigraphic information in the central part of the Limerick Syncline. It crosses a thick interfingering carbonate-volcanic sequence, intersecting the KKS, transitioning to the carbonates of the HBN, and exhibiting predominantly lavas and tuffs from 420 meters depth until the bottom.

Table 1 Drill hole information for petrophysical measurements with the formations intersected and the distance to the seismic profile LK-11-02.

DRILL HOLE	DEPTH (m)	TOTAL SAMPLES	DISTANCE TO LK-11-02	INTERSECTED FORMATIONS
TC-2531-001	926.6	199	144 m	KKS, HBN and KKR
TC-2638-004	440	50	430 m	WAL and ABL
TC-2638-008	605	51	430 m	WAL and ABL

https://doi.org/10.5194/egusphere-2025-2512
Preprint. Discussion started: 10 June 2025

TC-2638-026	349.6	50	120 m	WAL and ABL
TC-2638-036	352.5	39	78 m	WAL and ABL
TC-2638-074	389.5	50	20 m	WAL and ABL
TC-2638-088	677.3	50	297 m	LGG, WAL and ABL
TC-2638-101	461.3	50	195 m	WAL and ABL
G11-2531-01	520	84	4,890 m	KKS, HBN, KKR, LGG and WAL
G11-2638-06	518.6	88	1,830 m	LGG, WAL and ABL

Drill holes G11-2531-01 and G11-2638-06 (Fig. 1), located a few kilometres away from the seismic profile, provide important downhole petrophysical information about the stratigraphic sequence of the north and south flanks of the Syncline. Both drill holes cross the stratigraphy from the LGG to the ABL. G11-2531-01 intersects approximately 300 meters of interfingered volcanic and carbonate rocks before reaching the LGG.

3.2 Petrophysics data

Laboratory P-wave velocity (Vp) and density data were acquired for over 700 core samples, covering the full length of the available drill holes. Measurements were conducted on NQ-sized samples, each 10 centimetres in length. The sampling interval was planned based on the total drill hole length, aiming for approximately 50 samples per drill hole, except for TC-2531-001, G11-2531-01 and G11-2638-06, where denser sampling was carried out (Table 1). In addition to the laboratory measurements, drill holes G11-2531-01 and G11-2638-06 (Fig. 1) include legacy downhole sonic log data.

The Vp measurements were taken on dry core samples using a Proceq Pundit Lab ultrasonic pulse velocity device. Grain size variations in the samples can influence the pulse propagation. This effect can be minimised by selecting a frequency such that the wavelength is at least twice the size of the largest grains (Proceq Pundit Lab manual). In our study, the samples consist primarily of volcanic and carbonate rocks from the KKR, WAL and ABL (Fig. 2). A frequency of 150 kHz was selected, assuming a wavelength twice as large as the coarsest particles in the samples, such as fossils. Quality control was applied to the dataset, including filtering to retain only measurements with an accuracy greater than 75%.

The density measurements were taken on the same core samples, which were soaked in water for 24 hours before measurement, using an Ohaus Explorer balance equipped with an under-hook weighing system. Density is calculated using the Archimedes principle, which consists of weighing the sample in both air and water. The water temperature is considered in the calculation.

The legacy sonic log data from the two drill holes was acquired using full-waveform sonic probes. These probes employ dual transmitters and receivers to emit and detect high-frequency acoustic waves, measuring the first-arrival transit time of P-waves through the formation. The precise distance between the transmitters and receivers enables computation of the formation acoustic velocity (Robertson Geo Mining & Minerals).

3.3 Travel-time tomography

The tomographic velocity model was obtained from profile LK-11-02, using the PStomo_eq 3D local earthquake (LE) tomography algorithm (Benz et al, 1996; Tryggvason et al., 2002) that also handles the inversion of controlled source data (together and separately). The model is based on the legacy first arrivals picks used for statics corrections, which were complemented with new travel time picks for far offsets in this study. Forward modelling was performed by computing the time field from a source or receiver to all the model cells. Then, the travel times to source and receiver positions were calculated from the time field and the ray tracing was performed backwards and perpendicular to the isochrons (Tryggvason and Bergman, 2006). The inversion part of the processing is performed with the conjugate gradient solver LSQR (Paige and Saunders, 1982).

https://doi.org/10.5194/egusphere-2025-2512
Preprint. Discussion started: 10 June 2025

An appropriate initial velocity model is essential to ensure convergence during travel-time inversion. A smooth 2D model was developed in this study utilising a priori constraints from the petrophysical Vp data and drilling control on formation depths in the area. The model was generated from a set of 1D velocity profiles, incorporating shallow velocity estimates and a gradual increase in velocity with depth. The simplicity of the model was supported by the robustness of the inversion algorithm, which enabled effective use of these generalised velocity trends. Equally important is the accurate picking of first arrivals, which serve as the primary constraint for the tomographic inversion. Therefore, careful quality control and validation of the first-arrival times, including both legacy and new picks, were crucial to ensure the effective performance of the tomographic inversion. Inaccurate or inconsistent picks can lead to significant errors in the velocity model, potentially hindering convergence and reducing the reliability of the results.

3.4 Seismic imaging

3.4.1 Legacy seismic data available

The available legacy data of the 10.9 km long line LK-11-02 was acquired using a split-spread geometry with a Vibroseis seismic source, featuring a 20-meter source spacing and a 10-meter receiver spacing. The seismic data available consists of two datasets (Fig. 3): i) the raw data, and the processed stack and post-stack time migration delivered to Teck Resources Limited by Velseis Processing Ltd. and available at the Ireland Exploration and Mining Division, referred to in the section as legacy dataset 1; and ii) CDP gathers (containing geometry, statics correction, and de-noising), stack and pre-stack time migration, processed by Earth Signal Processing Ltd. (ESP) and available for this study through Group Eleven Resources, which is referred to as legacy dataset 2. This study uses these two legacy datasets as starting points for the new processing workflow.

While standard seismic pre-processing techniques were applied, this study does not focus on their evaluation. Instead, it emphasises the impact of incorporating additional information into the velocity field, refining the velocity model and improving post-stack processing.

The historic processing workflows for the legacy datasets 1 and 2 are described in Table 2. Dataset 2 differs slightly from dataset 1 by applying a different pre-processing sequence to enhance the signal-to-noise (S/N) ratio in the raw data. In dataset 2, ESP reports the application of surface-consistent amplitude scaling to address variable source and receiver coupling, and residual scaling to enhance offset contribution and to preserve amplitudes in noisy areas. A different set of statics corrections was also applied by ESP, minimising travel-time distortions in the CMP gathers and improving the stack response. Other significant differences include the post-stack processing and the Kirchhoff pre-stack time migration, which was applied using 100% of the smoothed stacking velocities. The dataset 2 pre-processed CDP gathers (Table 2) are the input dataset for our new processing.

Table 2 Processing workflows of the legacy datasets available for the study. In this study, we use the first break picks from dataset 1 and the CDP gathers (containing geometry, statics correction, and de-noising) from dataset 2.

Legacy Dataset 1	Legacy Dataset 2
1. Trace editing	1. Geometry and QC
2. Geometry	2. Refraction analysis
3. Static computation: Datum: 200 m, replacement velocity 4500 m/s	3. Replacement statics: Datum: 0 m, replacement velocity 3500 m/s
4. Amplitude recovery	4. Trace editing
5. Fan filter, linear noise: 6-30 Hz	5. Exponential scaling
6. Deconvolution: 100ms operator	6. Amplitude scaling
7. Velocity analysis 1: Picks 500 m interval	7. Vibroseis designature

https://doi.org/10.5194/egusphere-2025-2512
Preprint. Discussion started: 10 June 2025

8. Static calculation and application 1
9. Velocity analysis 2:
   Picks 250 m interval
10. Static calculation and application 2
11. AGC: 300 ms
12. DMO:
    Velocity of 4000 m/s
13. Velocity analysis on DMO gathers
14. NMO:
    30% stretch mute
15. Stack
16. Migration:
    Phase shift using 100% of smoothed velocity
17. Band-pass filter: 40-18 140-72 Hz-dB
18. AGC: 300 ms

8. Fourier filter:
   0-1000 m/s velocity, 0-28 Hz frequency
9. Deconvolution: 5/8 – 130/150 Hz
10. Residual scaling
11. Velocity analysis 1:
    Picks 500 m interval
12. Surface consistent statics
13. Final velocity analysis:
    Picks 250 m interval
14. Coherent noise attenuation: 12 Hz cut-off
15. Spectrum analysis (shots)
16. Sort to CMP gathers
17. Migration
    Kirchhoff pre-STM using 100% of smoothed velocity
18. Spectrum analysis (gathers)
19. Final mute
20. Stack
21. Multichannel trace scaling
22. Filter: 25/40 – 65/75 Hz

3.4.2 New seismic data processing

Our seismic processing workflow is outlined in Table 3. It focused on improving the velocity analysis in the area and incorporating the new information into the seismic processing applied in our study.

The new workflow includes semblance velocity picking, normal moveout correction (NMO), CDP stacking, de-noising, and post-stack time migration. Our stacking velocity model is guided by petrophysics and tomographic results following the normal moveout correction. In qualitative terms, when both laboratory Vp and tomography indicate high velocities in the shallow carbonate units, the stacking velocity is adjusted to reflect these values, aligning both the geological setting and the need to flatten reflectors during the velocity analysis.

The velocities were picked at an interval of 250 m based on the interactive normal-moveout correction and guided by the average velocity model obtained from the tomographic inversion and petrophysical measurements. After quality control of the stack section, we applied an additional de-noising sequence including Butterworth filtering, time-frequency domain (TFD) noise attenuation and 2D spatial filtering to suppress remaining coherent and random noise. The last step in the processing sequence was a Kirchhoff post-stack time migration, intended to relocate dipping events to their correct positions, collapse diffractions, and increase resolution. Given the complex geology of the study area and the moderate data quality, we avoided adding unnecessary complexity to the velocity model. This decision was made to prevent potential challenges and instability in the Kirchhoff time migration, particularly when dealing with sharp velocity contrasts (Pu et al., 2021). For the same reasons, we opted for post-stack migration, as pre-stack migration would require a more detailed velocity model than the data or geology allows.

Table 3 Reprocessing workflow applied to the legacy dataset 2 pre-processed shot gathers.

New Processing

https://doi.org/10.5194/egusphere-2025-2512
Preprint. Discussion started: 10 June 2025

1.	Semblance velocity analysis Picks 250 m interval
2.	NMO 30 % stretch mute
3.	Stack
4.	Butterworth filter: 12/17 – 50/100 Hz
5.	FTD noise attenuation 100 ms window, 5-70 Hz frequency
6.	2D spatial filtering
7.	Migration Kirchhoff post-STM using 100% of velocity

4 Results

4.1 Velocity analysis

P-wave velocities were first measured on the core samples from drill holes G11-2531-01 and G11-2638-06, which were then compared with the downhole sonic logs to analyse the correlation between the values obtained from both methods. To address the difference in sampling rates between the datasets (i.e. every 1 cm in the sonic logs vs every 10 m on average in the core samples), we resampled the sonic log curve to a coarser resolution, keeping values anchored at depths corresponding to laboratory measurements (Fig. 4). The methods displayed similar trends for Vp, although the sonic logs showed slightly higher velocities than the laboratory measurements. The discrepancies are likely due to differences in the sampling conditions (e.g. lithostatic vs atmospheric pressure, fresh rock vs degraded by time core samples), pore fluid (laboratory measurements were done on dried samples), and equipment frequencies. Nevertheless, the good correlation between the two datasets provided the confidence to extend our sampling campaign to the remaining eight drill holes and acquire velocity information from various locations along the seismic profile, an important step given that downhole petrophysical data is rarely available in mineral exploration.

The laboratory Vp dataset, comprising a total of 640 measurements, was categorised according to the main stratigraphic units as well as the main lithologies and textural characteristics (Fig. 5). Variations in velocity within carbonate rocks are closely related to porosity and pore types, with frame-forming pores generally associated with higher velocities (Eberli et al., 2003). Accordingly, the carbonate samples were classified as mudstone, wackestone, packstone, or grainstone. Samples with significantly increased clay content or the presence of chert were classified as argillaceous and cherty, respectively. In addition, features such as dolomitization, brecciation and mineralisation were included in the textural classification. Dyke and volcanic samples were also differentiated. However, their textures are not examined in detail in this study.

The Vp values of the units in the Limerick Syncline range from 3000 to 6500 m/s. The samples of the KKS identified as dykes and lithic tuffs show a wide range of P-wave velocities (from 3000 to 6000 m/s with a median around 4800 m/s). Intense clay alteration, possibly due to weathering, is a common characteristic amongst the KKS samples and is responsible for decreasing Vp to velocities close to 3000 m/s. The velocity for the KKR ranges from 4600 m/s to 6300 m/s (median of 5600 m/s), and the outliers displaying low velocities correspond mostly to volcaniclastic or tuff samples. The KKR also shows large variations in velocity due to its highly variable package of volcanic rocks, containing lava flows, tuffs and carbonate-rich pyroclastic flows, as per drill core observations.

https://doi.org/10.5194/egusphere-2025-2512
Preprint. Discussion started: 10 June 2025

The carbonate units show higher overall velocities compared to the volcanic rocks. Velocity outliers observed in the carbonate sequence can be related to increased clay content, dolomitization, brecciation and mineralisation, individually or combined. The packstones and coral-rich intervals of the HBN show higher velocities with a median value of 6100 m/s, while intervals dominated by wackestones display lower velocities and a median value of 5900 m/s (Fig. 5b). Outliers in this unit represent volcanic layers interbedded in the HBN limestone sequence.

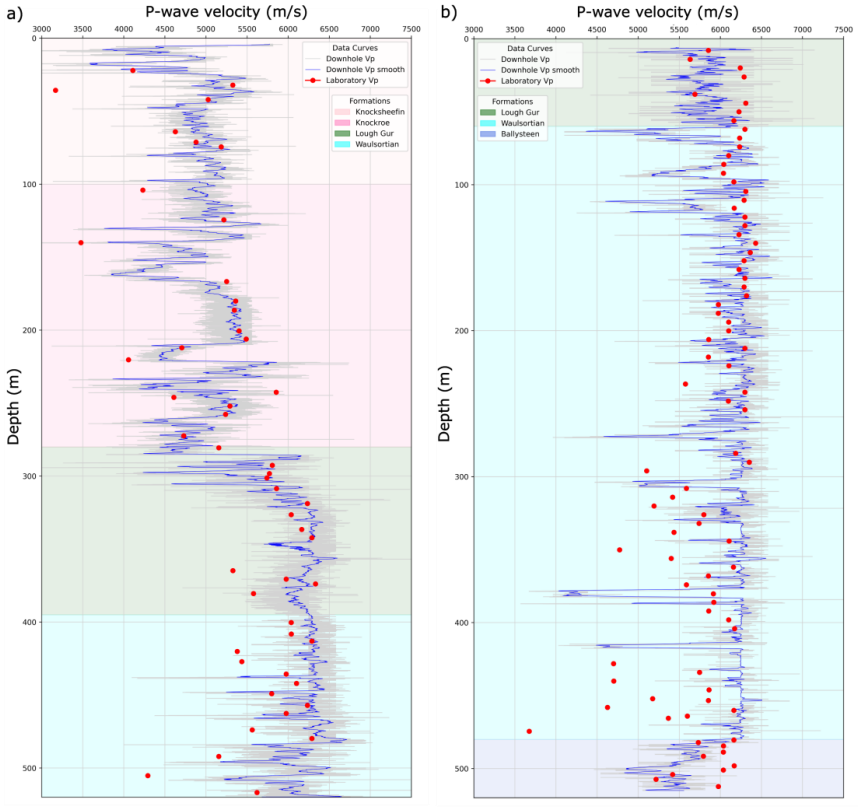

Figure 4: Comparison of downhole and laboratory P-wave velocity data a) for drill hole G11-2531-01, and b) for drill hole G11-2638-06. The light grey curve represents the downhole data, the blue curve represents the resampled downhole data, and the red dots represent the laboratory data. The background colours represent stratigraphic units intersected by the drill holes.

The LGG is composed of three different facies (Strogen, 1988) that can be identified throughout the samples: a bioclastic chert-rich wackestone, a poorly sorted crinoidal grainstone with rare chert and a non-argillaceous, well-washed grainstone. The higher velocities in the unit (6000 m/s) relate to the samples of non-argillaceous grainstone and chert-rich wackestone. In comparison, low velocities (5800 m/s) are associated with core samples with increased clay content.

The samples of the WAL show a wide range of velocities (Fig. 5). The unit comprises stacked microbial mud mounds with two main facies (Lees et al., 1995). One facies, representing the mud mound core, contains massive mudstones often with stromatactis cavities typically infilled with calcite. The other facies represent flanks of the mud mounds, which are composed of interbedded bioclastic wackestones, packstones and grainstones with variable amounts of wispy argillaceous material. The WAL is also frequently affected by post-depositional processes: it is the main host to Zn-Pb mineralisation and locally shows strong but chaotic dolomitization and brecciation textures, which are all commonly found in the samples. For this unit, velocities range from 3700 to 6500 m/s with a median around 6000 m/s, where increased clay content, dolomitization, and brecciation are common characteristics observed in the low spectrum of the velocity range. Higher velocities (around 6200

https://doi.org/10.5194/egusphere-2025-2512
Preprint. Discussion started: 10 June 2025

m/s) are predominant in the mud mound core facies samples. Intensely dolomitized samples exhibit lower average velocities (around 6000 m/s) with outliers well below 5000 m/s. Dolomitized samples show a wide range of velocities (3700 to 6500 m/s; Fig. 5b), likely reflecting the presence of various types and generations of dolomite. This reflects the observations of Blaney and Redmond (2015), who describe three textural types of dolomites in the WAL in the study area. Brecciated and mineralised samples show velocities ranging from 4700 to 6400 m/s, with a median value of 5800 m/s, and from 5500 to 6400 m/s, with a median of 6100 m/s, respectively. The decrease in velocity relative to the surrounding host rocks caused by these processes appears to depend on the hydrothermal alteration intensity. Intensely brecciated samples show lower velocities than weakly brecciated ones. The high median value in mineralised samples is attributed to the more common presence of pyrite, which exhibits higher velocities than sphalerite and galena. This analysis is also reported by Salisbury et al. (2000). Mineralisation and the WAL mudstone show similar velocities (Fig. 5b).

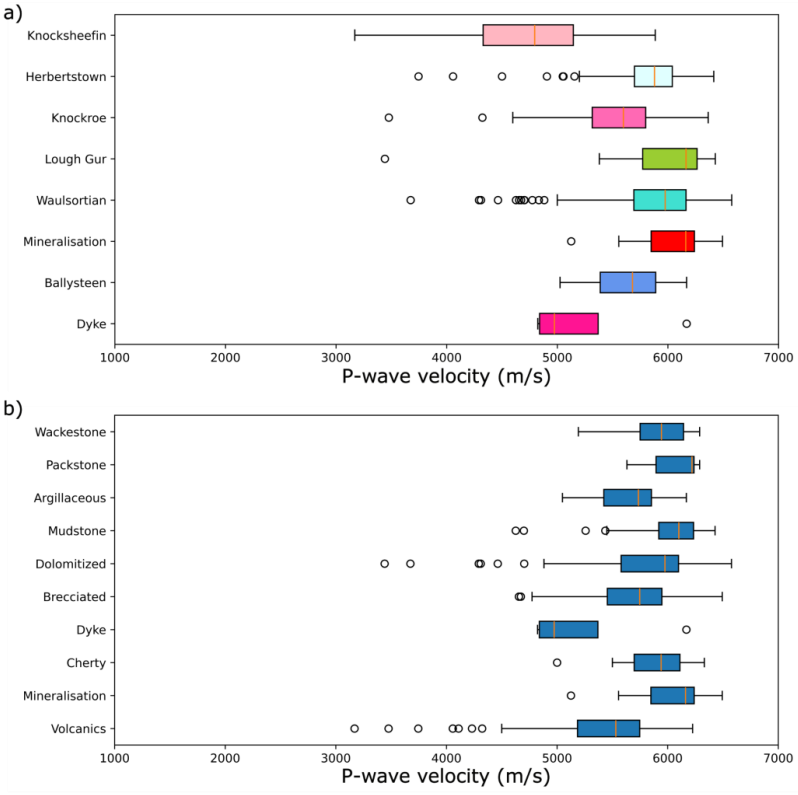

Figure 5: Box plot of the laboratory P-wave velocity data. Median values are represented by the orange line, box length and whiskers vary according to the interquartile range. Outliers are represented by circles. a) Data classified according to the main stratigraphic units in the Limerick Syncline, and b) data classified according to lithology.

The ABL samples display the lowest velocities of the carbonate sequence, ranging from 5000 to 5800 m/s, with a median of 5700 m/s. This is consistent with the argillaceous bioclastic content of the limestones, with overall clay content representing approximately 30% of the lithology (Sleeman and Pracht, 1999). Clay-rich samples reveal velocities between 5000 and 6100 m/s and a median value of 5800 m/s (Fig. 5b).

Overall, the velocity contrasts within the stratigraphic units of the Limerick Syncline are very mild. Notable velocity contrasts can be seen in the contact between the volcanic-dominated (KKR and KKS) and the carbonate-dominated (LGG and WAL) units, and between the WAL and the ABL (Figs. 4 and 5).

https://doi.org/10.5194/egusphere-2025-2512
Preprint. Discussion started: 10 June 2025

To extend and validate the Vp petrophysical measurements over the entire study area, we performed travel-time tomography by inverting first-arrival picks from legacy dataset 1, resulting in a P-wave velocity model (Fig. 6). The velocity field was resolved up to a maximum depth of 245 m. The resolution in travel-time tomography is strongly constrained by the available offsets and the seismic velocities involved in the inversion, which determines the final ray coverage used to plot the velocity models. For this reason, new picks for far offsets were included in the inversion, although these were limited because of the low S/N ratio in some of the acquired seismic reflection data.

The uppermost layer in the model shows a low-velocity zone (purple to blue colours, ≤ 2000 m/s) with a thickness ranging from 10 to 50 m, which can be correlated with the overburden in the area according to core logging data. Below the immediate overburden, a thick low-velocity zone (≤ 3500 m/s) appears in the centre of the profile, south of 146000mN, thickening up to 170 meters close to drill hole TC-2638-088, and reducing in thickness around 144000mN. These lower velocities correspond to altered volcanic rocks from the KKS and KKR units in TC-2531-001 (0 to -60 m MSL) and TC-2638-088 (30 to -60 m MSL). Laboratory measurements for these intervals also reveal relatively reduced velocities between 4700 and 5900 m/s and 4800 and 5400 m/s, respectively.

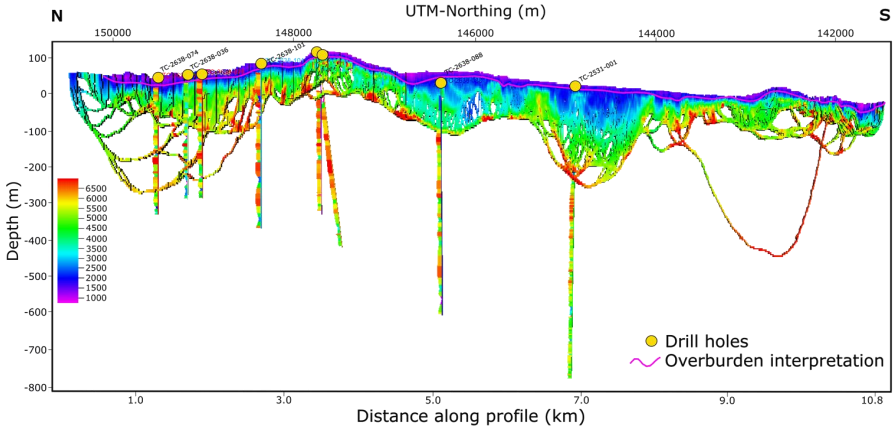

Figure 6: Travel-time tomography model displaying P-wave velocity data alongside petrophysical velocity measurements from the drill hole samples (marked by the yellow circles). The purple line outlines the overburden thickness interpreted from the model and drill hole data.

Zones of highly porous limestones with visual evidence of cavitation are seen from 0 to -60 m MSL in drill holes, indicating greater depths than usual in karst-related features in this area. Karstification is common in the KKR and the limestones of the LGG and WAL, as well as along fault zones (McCormack et al., 2017; O'Connell et al., 2018).

Zones of higher velocities ranging from 4000 to 6500 m/s are present near the surface on the northern and southernmost sides of the profile and underlying the central low-velocity zone (Fig. 6). On the north side of the profile, this corresponds with the presence of the WAL at the surface, which is well-constrained by drilling. Drill hole TC-2638-101 shows similar elevated laboratory velocities to the velocity model (from 70 to -100 m MSL), ranging from 6000 to 6300 m/s, exhibiting a grey dolomite. These depths correspond to a sequence of nearly completely dolomitized WAL mud mounds. Similarly, dolomitization also affects WAL mud mounds in drill hole TC-2638-036 at similar depths. This sequence reveals lower velocities (5700 to 6000 m/s), corresponding to a brownish dolomite. This strongly suggests that the tomographic velocity model responds to different dolomitic textures. High velocities can also be associated with the stromatactis textures present in the core facies of the WAL mud mounds, and these are intersected by the drill holes TC-2638-074 and TC-2638-101, displaying velocities of 6000 m/s on both the model and drill holes.

The velocity model shows interfingered low and moderate velocity zones around 146000mN (Fig. 6), corresponding to 90 meters of altered volcanic sequence of KKR underlain by a dolomitized zone of the LGG intersected by drill hole TC-2638-

https://doi.org/10.5194/egusphere-2025-2512
Preprint. Discussion started: 10 June 2025

088. South of 144000mN, the same units are exposed at the surface, with the model revealing a thinner upper low-velocity layer and predominantly high velocities below, indicating a distinct velocity response compared to the northern section of the model. The bedrock geology in this area (Fig. 1) is mapped as KKR.

Younger units (KKS and HBN) are exposed between 146000mN and 144000mN. The response in this portion of the tomography exhibits chaotic behaviour with increased lateral velocity variability, interpreted as interfingering between the volcanic- and limestone-dominated intervals, as supported by drill hole TC-2531-001. The upper 200 meters of this drill hole intersect an interfingered sequence of thickly bedded volcanics, argillaceous limestone, cavities and basaltic intrusions. Laboratory Vp ranges from 4700 to 6200 m/s, aligning well with velocities observed in G11-2531-01 (Fig. 4a), which also intersects KKS, KKR and the limestones of LGG.

4.2 Acoustic impedance

By combining the velocity analysis with density data from the core samples, we calculated the acoustic impedance of the main stratigraphic units and lithological types observed in the drill holes (Fig. 7).

Velocity contrasts between individual units within the Limerick Syncline are generally mild. The most notable differences occur between the WAL and ABL (mean velocities of 6000 vs 5500 m/s, respectively, representing a 10% contrast) and between the LGG and the KKR (mean velocities of 6000 vs 5600 m/s, respectively). These velocity differences are also observed in the downhole Vp logs (Fig. 4). Density contrasts are most prominent between the carbonate and volcanic rocks (approximately 2.7 vs 2.9 g/cm^3, respectively) and the carbonate and mineralisation (2.7 vs 3.0 to 4.2 g/cm^3, respectively).

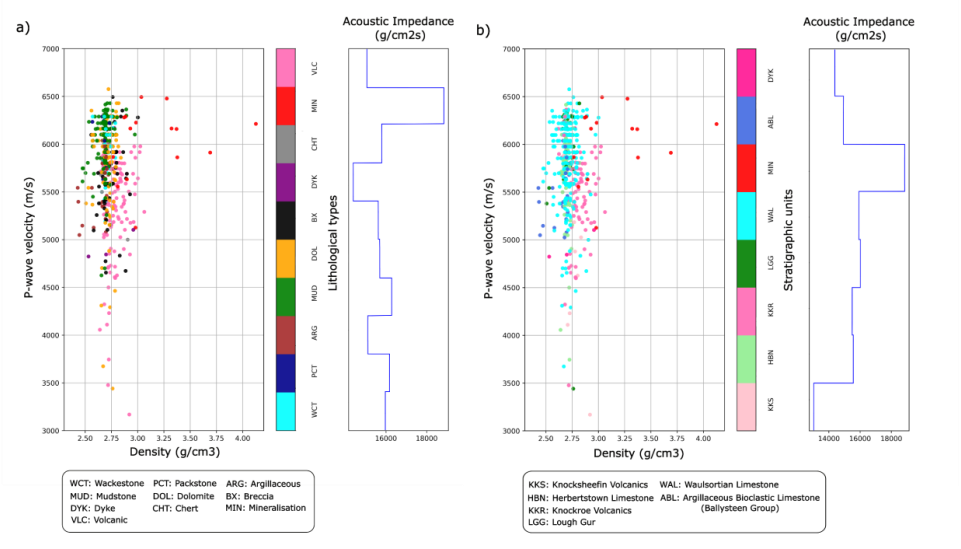

Figure 7: Laboratory P-wave velocity and density data cross-plot. Data points coloured according to a) lithology, and b) main stratigraphic units. The mean acoustic impedance per lithology/unit is outlined in blue.

The ABL exhibits lower acoustic impedances (around 15,000 g/cm^{2}s) than the micritic mudstone samples of the WAL (around 16,500 g/cm^{2}s). This reflects the lithological composition of the upper ABL, containing significant portions of laminated and wavy argillaceous mudstone. Where the two units are juxtaposed, an impedance contrast of 1,000 to 1,500 g/cm^{2}s is expected. However, as seen in G11-2638-06 (Fig. 4b), the transition between these units can be gradual, with the top tens of meters of the ABL representing an argillaceous nodular micrite unit often transitional to the WAL (Somerville et al., 1992). As expected, acoustic impedance in the WAL is highly variable, due to significant variation in density and velocity (Figs. 5 and 7b). Most

https://doi.org/10.5194/egusphere-2025-2512
Preprint. Discussion started: 10 June 2025

micritic mudstone samples in the WAL show high acoustic impedance, contrasting with the brecciated and dolomitized samples in the unit (≤ 15,500 g/cm^{2}s).

The acoustic impedance in the LGG gradually decreases upwards (e.g. G11-2638-06 in Fig. 4b), however, it is mostly indistinguishable from the WAL. The KKS shows very low acoustic impedance (around 13,000 g/cm^{2}s). It is characterised by basaltic lava flows, intrusions and tuffs, representing thick massive homogeneous units (Strogen, 1983). Intense chlorite-clay alteration is common in most of the measured KKS samples, typical of extrusive units in both KKS and KKR (Slezak et al., 2023). This may explain the observed low overall acoustic impedance (13,000 g/cm^{2}s) and low velocities (Figs. 4a and 5a). Basaltic samples of the KKR show much higher acoustic impedance, mainly between 15,000 and 16,000 g/cm^{2}s, and they are distinctly dense (between 2.75 and 3.00 g/cm^3; Fig. 7b). The KKR samples are dominated by relatively unaltered fine-grained massive basalt intrusions, and lower values within KKR (13,500 g/cm^{2}s) correspond to volcaniclastic and tuff samples, which are often altered. The HBN shows very similar behaviour to LGG and WAL, and when interfingered with KKR, does not show notable acoustic impedance contrasts.

Massive sulphide mineralisation shows the highest acoustic impedance values (≥ 20,000 g/cm^{2}s) due to the densities associated with pyrite, sphalerite and galena, with an expected impedance contrast of 4,000 to 5,000 g/cm^{2}s for mineralised WAL.

4.3 Seismic reprocessing

The velocity analysis provided key information to reconstruct the velocity field in the study area, which informed the new stacking velocity model used in both the stack and post-stack time migration.

Based on the picked stacking velocity after analysing the seismic data, a new stack of line LK-11-02 was obtained (Fig. 8). The reprocessed seismic image features areas with prominent reflectivity. The northern part of the profile contains the Stonepark Zn-Pb prospect (Fig. 1), with several drill holes drilled to at least 300 meters (CDPs 0-600). This area is characterised by a group of high amplitude reflections (R1) with variable geometries and lateral continuity between 100 and 300 ms, exhibiting mound-shaped structures with greater impedance contrasts than those observed right below. Towards the south, a sequence of gently to moderately dipping reflections (R2) shows high amplitude and subparallel to mound-shaped geometries. These reflections are also observed between the CDPs 720 and 1130 and between 1130 and 1335, around 300 to 500 ms (Fig. 8).

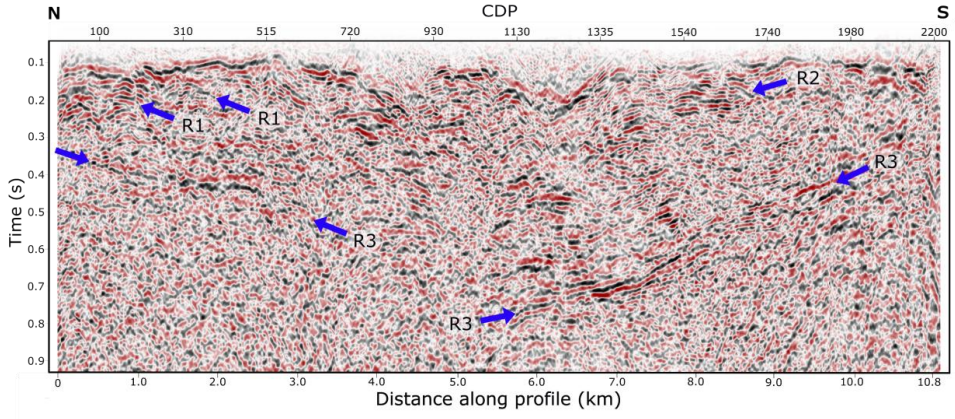

Figure 8: P3 two-way time stack section with reflections R1, R2 and R3 highlighted by blue arrows.

Laterally continuous reflections (R3) are identified on both sides of the section. The R3 reflections are the deepest continuous reflectors in the profile, below which the reflections become more incoherent. However, there is a significant discontinuity at the central part of the section (between CDPs 720 and 1130), interrupting the R3 package. Notably, these R3 reflectors dip in

https://doi.org/10.5194/egusphere-2025-2512
Preprint. Discussion started: 10 June 2025

opposite directions across this discontinuity (Fig. 8). South of the discontinuity, between CDPs 1130 and 1740, the reflections exhibit good continuity again, with subparallel internal geometries and moderate to steep dips.

5 Discussion

The acquisition and processing of additional velocity field information provided a key hitherto missing step, enabling petrophysics-guided seismic reprocessing of legacy data in the Limerick Syncline. The Vp data collected from drill holes along the profile LK-11-02 and the results of the travel-time tomography presented insights into the P-wave velocity of the main geological units of the shallow part of the study area, allowing us to improve and reinterpret the seismic image.

5.1 Seismic interpretation

Figure 9c shows an integrated seismic interpretation of the main stratigraphic units and structures, with time-converted drill holes containing geological logging information highlighting formations, dolomitization, brecciation, argillaceous intervals and dyke intrusions. The black dashed lines outline the interpretation of previously unknown faults F1 and F2. The coloured top bar represents the bedrock stratigraphy extracted from the geological map (Geological Survey Ireland, 2022).

The reflections R3 are interpreted to represent the LLS Group (yellow horizon in Fig. 9c), comprising interbedded cross-bedded sandstones, oolitic and skeletal grainstones and fissile shales with desiccation cracks (Somerville & Jones, 1985; Somerville et al., 2011). This heterolithic sequence could explain the observed seismic facies of a high-amplitude, subparallel, continuous package of reflectors. The top of these reflections is interpreted as the contact between the mixed siliciclastic-carbonate-evaporite sequence and the fully marine open ramp carbonate-dominated sequences, likely corresponding to the more argillaceous Ballymartin Formation, but certainly including the Ballysteen Formation (Somerville and Jones, 1985).

The enhanced continuity of reflections and the geological constraints from drilling data at the northern portion of the section facilitated the interpretation of the contact between the ABL and the WAL (outlined by the dark-blue horizon in Fig. 9c). The overlying zone (WAL) exhibits high-amplitude, mound-shaped structures with greater impedance contrasts than those observed right below (between 100 and 300 ms), corresponding with the observed variability in Vp with different facies within the WAL.

Internal form lines within the WAL carbonate rocks (cyan blue in Fig. 9c) highlight various geometries outlined by moderate to high amplitude reflectors. These semi-continuous reflectors show mound-shaped geometries with opposing dip, and associated onlap and offlap terminations. These correlate well with changes in facies of the WAL mud mounds as observed in drill holes in Fig. 9c. Transition from core mudbank facies to flank facies correlates with increased reflectivity. The cores of the mud mound consist of massive micrite mudstone, with higher acoustic impedance, and the mud mound flanks consist of higher bioclastic content with variable amounts of clay, with lower acoustic impedance (Fig. 7). Outcrops studies and drill data across the Irish Midlands clearly show that individual WAL mud mounds can have dimensions of tens to a few hundred meters in thickness (Lees, 1964) with amalgamated mud mound complexes extending for kilometres (Devuyst and Lees, 2001), especially in the Limerick area (Somerville et al., 2012).

The very high amplitude and laterally continuous quasi-horizontal shallow reflectors seen north of CDP 720 at 100 ms (dark pink dashed form line; Fig. 9c), coincide well with observed low-angle basaltic dykes, as well as thick (≥ 50 meters) argillaceous-rich WAL mud mound flank facies in TC-2638-101, and thick argillaceous flank facies in TC-2638-026 and TC-2638-036.

Towards the south, several high-amplitude semi-continuous quasi-horizontal reflectors, like the R2 reflections (Fig. 8), were interpreted as dark pink form lines (Fig. 9c), representing the KKR. These strong reflectors are often underlain by extensive

https://doi.org/10.5194/egusphere-2025-2512
Preprint. Discussion started: 10 June 2025

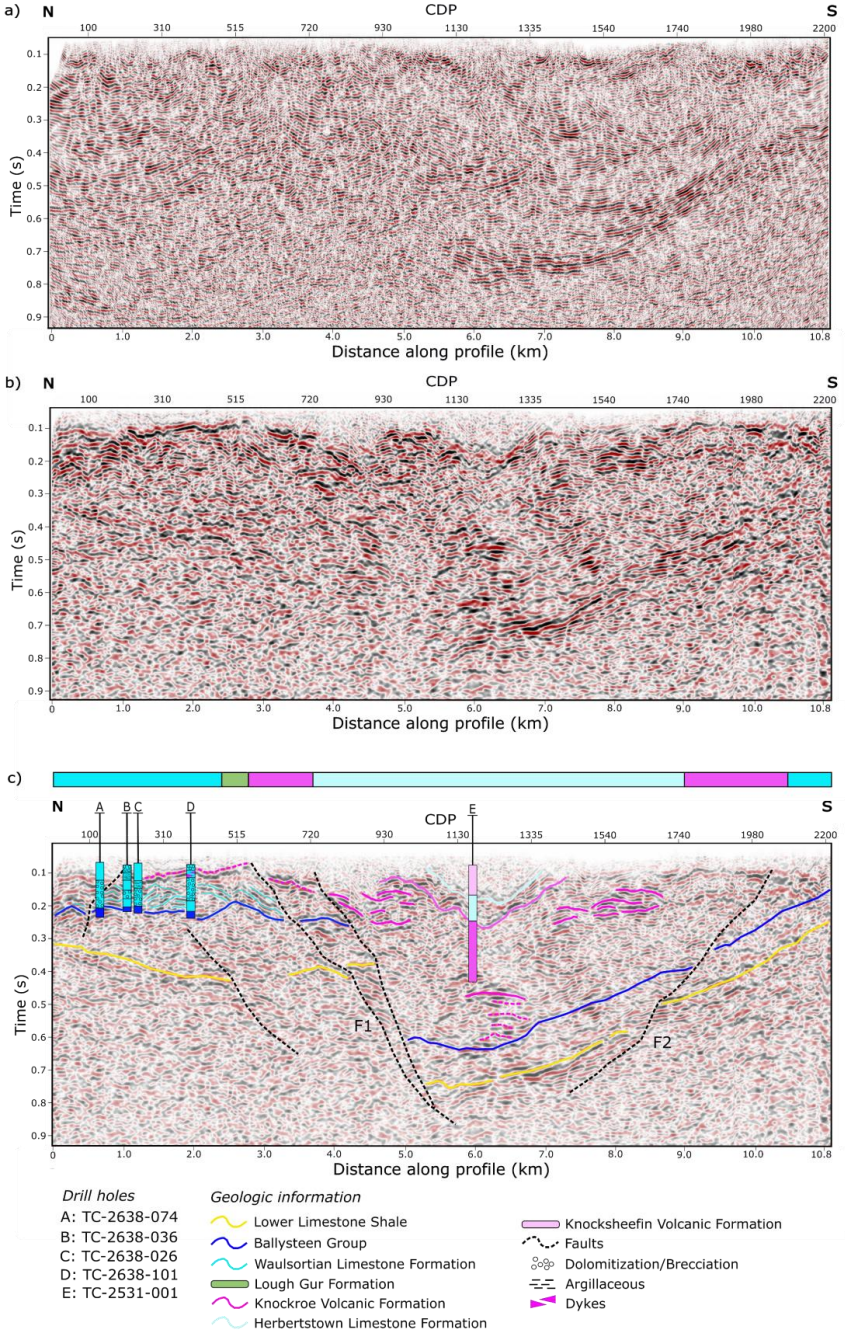

Figure 9: Legacy dataset 1 and new processing migrated sections. a) Legacy phase-shift post-stack time migration and b) new Kirchhoff post-stack time migration. (c) Seismic interpretation of the main stratigraphic units with time-converted drill holes containing geological logging information (units and textures - dolomitization/brecciation, argillaceous intervals and dyke intrusions). Interpretation of faults F1 and F2 are outlined by black dashed lines. The coloured top bar represents the bedrock stratigraphy extracted from the geological map

zones of moderate to high amplitude but discontinuous reflectivity, rooting down for up to 600 ms. Laterally, these reflections are interfingering with chaotic reflections of lower amplitude. The KKR comprises abundant basaltic maar-diatremes, lava flows, intrusions, tuffs and volcaniclastic units (Strogen, 1983; Elliott et al., 2015; Slezak et al., 2023). The high-amplitude,

https://doi.org/10.5194/egusphere-2025-2512
Preprint. Discussion started: 10 June 2025

mound-shaped reflections between CDPs 1130 and 1335 are therefore interpreted as an example of an intrusion (possibly a diatreme pipe and associated intrusives) associated with the KKR. The chaotic low-amplitude reflections between 150 and 400 ms are interpreted as interfingering between the different volcanic rocks and the carbonate rocks of the LGG and HBN.

The contact between the KKS and the HBN is constrained by the drill hole TC-2531-001 and outlined by the light-green horizon (Fig. 9c). The acoustic impedance plot (Fig. 7) exhibits low values for the altered volcanic samples, tuffs, and volcaniclastics and high values for basaltic lava flows, reinforcing the contrasts observed in the seismic section.

Several interpreted faults crosscut the section. A significant discontinuity interrupts the continuity and elevation of the LLS package. This is interpreted as a major south-dipping (segmented) fault (F1) displacing the LLS by approximately 450 ms. Additionally, a north-dipping fault (F2) is interpreted to the south of F1, displacing the LLS by approximately 100 ms. Reflectors of overlying units are dipping north towards F1, forming a clear normal fault half-graben geometry, with F1 representing a terraced fault system. Several antiformal geometries and domed reflections are observed in the immediate hanging wall and footwall of the fault, as well as in the F1 fault blocks. A zone of more steeply dipping LLS reflectors is also seen between CDPs 1540 and 1740. These are interpreted as representing inversion geometries, possibly associated with the Variscan Orogeny.

5.2 Legacy and new processing

To assess the impact of the updated velocity model on the imaging of profile LK-11-02, the results of the new Kirchhoff post-stack time migration (Fig. 9b) are compared against the legacy dataset 1, which consists of a phase-shift post-stack time migration (Fig. 9a).

The new post-stack time migration demonstrates good signal recovery in both the shallow and deep portions of the section, revealing enhanced continuity and previously unresolved reflections of geological significance. While the legacy phase-shift time migration exhibits parts of reflections like R1, between CDPs 100 and 200, and R3 at 400 ms, it struggles to resolve other reflections recovered in the new processing. Reflections R3 are visible in the southern part of the profile (south of CDP 1130) in both workflows, with good continuity. Moderately dipping reflectors between CDPs 1540 and 1740, within two-way times of 400 to 500 ms, are well imaged in the legacy migration (Fig. 9a), but lose continuity in the new processing. Despite this, similar onlap terminations are evident in both images near CDP 1540. Apparent migration smiles in the legacy image are collapsed in the new processing, leading to improved imaging, particularly in the shallow zones below the KKS (Figs. 9b and 9c). Overall, the new migrated section enhances reflector geometries and amplitude variations, making the image more interpretable.

5.3 Implications for mineral exploration

According to Salisbury et al. (2000), a sulphide deposit can be imaged using seismic if it meets three conditions: i) a sufficiently high reflection coefficient (R), specifically greater than 0.06 in their study; ii) a diameter greater than the width of the Fresnel zone; and iii) a thickness of at least ¼ wavelength due to seismic vertical resolution.

In our study, although the Zn-Pb mineralisation in the Limerick Syncline has a sufficiently high reflection coefficient and Fresnel zone, it is unlikely to be directly imaged due to its moderate thickness. The mineralisation typically occurs in 10-meter intervals within brecciation zones in the WAL, below the vertical resolution of the seismic data (approximately 40 meters). However, our acoustic impedance study indicates that the mineralisation exhibits the highest impedance values compared to the main lithologies in the area (Fig. 7). This suggests that if a sphalerite/galena-rich zone extended laterally for at least 240 meters (approximate Fresnel zone width) and had a minimum thickness of 36 meters, it could potentially be imaged by the seismic (calculations assume Vp = 5800 m/s and a depth of 200 meters).

https://doi.org/10.5194/egusphere-2025-2512
Preprint. Discussion started: 10 June 2025

Brecciation zones are also extensively present in the Stonepark WAL, showing lower acoustic impedance values compared to unaltered carbonate samples (Fig. 7). This contrasts with the seismic characteristics of WAL mud mounds. Drill holes intersected breccias between CDPs 100 and 515, within two-way times of 100 and 200 ms (Fig. 9c), providing constraints for the seismic interpretation. These brecciated zones coincide with chaotic, low-amplitude seismic facies. Dolomitization occurs in the same area at different intervals, however, its seismic facies closely resemble those of the mud mounds.

The distinct seismic facies observed in brecciated zones, as confirmed by drilling, highlights the potential for using brecciation as a seismic proxy for targeting mineralisation. This approach could also support drilling campaign planning. To further evaluate its effectiveness, we will apply this reprocessing workflow to the other five Stonepark and Pallas Green seismic profiles in the future.

5.4 Implications for the architecture of the Limerick Syncline

The Limerick Syncline forms a regional ovoid-shaped map pattern whose structural evolution remained poorly understood. The Stonepark and Pallas Green deposits, located in the northwest portion of the Syncline, are crosscut by a series of small throw, north-northwest-striking faults that appear to locally control the distribution of mineralisation (Blaney and Coffey, 2023) but which lack demonstrable growth sequences. However, the main basin-controlling and potentially ore-controlling normal faults remained unidentified in the study area (Blaney and Redmond, 2015). A key implication of the new processing is that such major faults (F1, F2) are now clearly identified.

A considerable change in thickness is observed in the stratigraphy from north to south of the profile (Fig. 9). The units are crosscut by various faults along the section (Fig. 9c), including the major south-dipping fault (F1) and the north-dipping fault (F2). No significant thickness changes are observed in the Early Mississippian units, LLS and ABL. However, the thickening of the KKR volcanic sequence in the hanging wall of F1 indicates potential fault activity during the Late Tournaisian to Early Viséan, corresponding to the KKR and KKS emplacement (Slezak et al., 2023). This timing is also observed in the northern and central Midlands of Ireland, where faults are suggested to have been active during the Upper Tournaisian and have influenced basin and mineralisation development (Johnston, 1999; de Morton et al., 2015).

The south-dipping fault (F1) displays a segmented geometry showing gentle rotation of the reflectors between the two interpreted segments (CDPs 515 to 930). At the hanging wall and footwall of F1, domed reflections are interpreted as inversion geometries (Bonini et al., 2012) associated with the Variscan Orogeny deformation, which led to regional north-south compression and consequent basin inversion, reactivating normal faults and producing reverse faulting (Meere, 1995; Fusciardi et al., 2004; Kyne et al., 2019). Similar domed geometries are also observed on the south side of the profile, dipping towards fault F2. These geometries indicate the impact of the compressional event in the Limerick Syncline.

In addition to identifying faults, the new processing has also enhanced our understanding of the distribution of the volcanic sequence along the seismic profile, which shows some association with faulting. The interpreted low-angle basaltic dykes, located north of CDP 720 (Fig. 9c), are interrupted by the segmented fault (F1). This high-amplitude reflector package reveals an increased thickness between CDPs 515 and 720, in comparison to the geometry observed north of CDP 515, suggesting the coeval timing of faulting and volcanism in the region. High-amplitude and laterally continuous quasi-horizontal shallow reflectors, such as those linked to the basaltic dykes, are also noted south of CDP 1740 around 100 ms, intersected by fault (F2). This indicates that the southern side of the profile displays a geological setting very similar to that of the northern side, where the Stonepark deposit is situated.

https://doi.org/10.5194/egusphere-2025-2512
Preprint. Discussion started: 10 June 2025

5.5 Velocity analysis

The P-wave velocity shown in Fig. 6, from travel-time tomography, details the near-surface of both sides of the Limerick Syncline. The low velocity zone associated with the overburden and karstification on the north side shows greater thickness than the south side, which shows a more rapid increase in velocity. However, thickening of this low velocity zone is observed towards the end of the profile, south of 142000mN, which potentially indicates limestone or fault-related karstification. The performed velocity analysis showed that the Waulsortian Limestone Formation can be very complex due to its variable lithologies and consequent wide range of velocities, which is controlled by the mud mound facies, clay content, dolomitization, brecciation and mineralisation. As confirmed by the drill hole data, the dolomitization is widespread in the Stonepark deposit and replaces extensive areas of the Waulsortian Limestone, influencing the velocity model. Coincidentally with Stonepark, we observe lower velocities in the model where drill holes intersected intense dolomitization and brecciation, processes that can decrease Vp as seen in the petrophysics data.

This interpretation is more challenging on the south side of the profile because of the absence of drill holes. The rapid increase in velocity in areas predominantly composed of Waulsortian Limestone could indicate either the presence of clean micritic Waulsortian or high-velocity dolomite. The same lateral velocity contrast of high and moderate velocity zones seen between 150000 and 148000mN on the north side, coinciding with different dolomite textures and brecciated zones in Stonepark, is also seen between 144000 and 142000mN on the south side of the velocity model. Interestingly, the south side of the seismic section suggests the presence of a major north-dipping fault (Fig. 9c), which could have acted as a hydrothermal fluid conduit, emplacing mineralisation in the WAL on the opposite flank of the Limerick Syncline.

6 Conclusions

This study demonstrates the impact of selecting an appropriate processing workflow and integrating geological and petrophysical data on enhancing legacy seismic data. Incorporating additional datasets such as drilling information, downhole and laboratory P-wave velocity measurements, and travel-time tomography improved the subsurface imaging of the profile LK-11-02. The velocity and acoustic impedance analysis provided valuable insights into the imaging potential of unit boundaries, brecciation zones and mineralisation. The reprocessed seismic section improved the interpretability of lateral lithology changes, such as the interfingering of volcanic and carbonate rocks and fault zones, previously considered gaps in the subsurface understanding of the area. We interpreted a south-dipping fault zone, which can be part of the conduits that provided the mineral system with metal-bearing hydrothermal fluids. And, from the acoustic impedance analysis, we observed that the mineralisation has a high reflection coefficient. However, in the Limerick Syncline, the mineralised intervals are not thick enough to be directly imaged with the available seismic data resolution.

Furthermore, this study raises considerations regarding the southeastern side of the Limerick Syncline, where seismic data revealed a major north-dipping fault, and similarities in velocity distribution observed in the travel-time tomography suggest a potentially similar setting of the carbonate rocks, emphasising the need for further investigation with a focus on mineralisation potential.

Lastly, the workflow explored in this study presents a cost-effective approach for mineral exploration. By revisiting the legacy seismic data and integrating complementary techniques into the reprocessing, valuable new insights can be extracted, offering an alternative to, or supporting the decision to, acquire new seismic data. Moreover, this approach enables the recovery of additional geological information from datasets that required significant financial and operational effort to acquire, thus contributing to the revalorisation of existing resources and maximising their exploratory potential.

https://doi.org/10.5194/egusphere-2025-2512
Preprint. Discussion started: 10 June 2025

Data availability

Seismic data underpinning this work can be requested through the Geoscience Regulation Office (GSRO) of the Department of the Environment, Climate and Communications of the Government of Ireland. The petrophysics data generated in this work can be obtained upon request from the authors and will be published in a research repository (Zenodo). Other complementary data can be obtained from the authors upon request.

Author contributions

VS: conceptualisation, petrophysical data acquisition, seismic, tomography and petrophysical data processing, data interpretation and integration, writing (original draft preparation) and editing; **AM:** conceptualisation, project management, supervision, funding acquisition, reviewing; **KT:** conceptualisation, data interpretation and integration, supervision, reviewing; **JA:** seismic processing methodology, supervision, reviewing; **DM:** travel-time tomography methodology, supervision, reviewing; **RB:** seismic processing methodology, reviewing.

Competing interests

The authors declare that they have no conflict of interest.

Acknowledgements

We greatly thank Group Eleven Resources, particularly Mark Holdstock and Sean Walsh, for providing geological logging data and drill core samples used in this study for laboratory petrophysical measurements, as well as for valuable geological discussions. We also acknowledge Robertson Geo for downhole petrophysics data acquisition. We are grateful to Glenn Morgan, Earth Signal Processing, and VelSeis Processing for providing the legacy seismic datasets used in the new processing discussed in this study. Additionally, we appreciate AspenTech, RadExPro and SLB for granting academic licenses for their software, which is used as the main tool in seismic processing. Special thanks to Philip Rieger and Eoin Dunlevy for their invaluable support in geological discussions. Finally, we extend our gratitude to the Geological Survey of Ireland for hosting the UCD Petrophysics Laboratory from 2021 to 2023 and to research assistants Conor Farrell, Eoin Byrne and Gabriel Cavalcanti for their valuable support in the petrophysics laboratory.

Financial support

This research was partly supported by a UCD Ad Astra Studentship and partly supported by Science Foundation Ireland, now Research Ireland, projects 13/RC/2092_P2 and 16/RP/3849. JA and DM acknowledge funding from the VECTOR project; this research has received funding from the European Union's Horizon Europe research and innovation programme under grant agreement no.101058483 and from UK Research and Innovation.

References

Alcalde, J., Carbonell, R., Pospiech, S., Gil, A., Bullock, L.A. and Tornos, F., 2022. Preface: State of the art in mineral exploration. *Solid Earth*, *13*(7), pp.1161-1168.

Ali, S.H., Giurco, D., Arndt, N., Nickless, E., Brown, G., Demetriades, A., Durrheim, R., Enriquez, M.A., Kinnaird, J., Littleboy, A. and Meinert, L.D., 2017. Mineral supply for sustainable development requires resource governance. *Nature*, *543*(7645), pp.367-372.

https://doi.org/10.5194/egusphere-2025-2512
Preprint. Discussion started: 10 June 2025

Ashton, J.H., Beach, A., Blakeman, R.J., Coller, D., Henry, P., Lee, R., Hitzman, M., Hope, C., Huleatt-James, S., O'Donovan, B. and Philcox, M.E., 2018. Discovery of the Tara Deep Zn-Pb Mineralization at the Boliden Tara Mine, Navan, Ireland: Success with Modern Seismic Surveys.

Bell, T., Turner, G., Bhat, G. and Knell, B., 2023, August. Multiscale insights into the Mount Weld REE deposit from 2D and 3D active seismic survey data. In *SEG International Exposition and Annual Meeting* (pp. SEG-2023). SEG.

Benz, H.M., Chouet, B.A., Dawson, P.B., Lahr, J.C., Page, R.A. and Hole, J.A., 1996. Three-dimensional P and S wave velocity structure of Redoubt Volcano, Alaska. *Journal of Geophysical Research: Solid Earth*, *101*(B4), pp.8111-8128.

Blaney, D. and Redmond, P.B., 2015. Zinc-lead deposits of the Limerick Basin, Ireland. *Current Perspectives on Zinc Deposits*, pp.73-84.

Blaney, D. and Coffey, E., 2023. The volcano-stratigraphic setting of the Pallas Green Zn-Pb deposit, County Limerick The volcano-stratigraphic setting of the Pallas Green Zn-Pb deposit, County Limerick. In: Andrew, C.J., Hitzman, M.W. & Stanley, G. *Irish-type Deposits around the world,* Irish Association for Economic Geology, Dublin, pp. 285-308. DOI: https://doi.org/10.61153/QHKU2937

Bonini, M., Sani, F. and Antonielli, B., 2012. Basin inversion and contractional reactivation of inherited normal faults: A review based on previous and new experimental models. *Tectonophysics*, *522*, pp.55-88.

Cheraghi, S., Hloušek, F., Buske, S., Malehmir, A., Adetunji, A., Haugaard, R., Snyder, D. and Vayavur, R., 2023. Reflection seismic imaging across a greenstone belt, Abitibi (Ontario), Canada. *Geophysical Prospecting*, *71*(7 Special Issue: Mineral Exploration and Mining Geophysics), pp.1096-1115.

Chew, D.M., Stillman, C.J., Holland, C.H. and Sanders, I.S., 2009. Late Caledonian orogeny and magmatism. *The Geology of Ireland*, *2*, pp.143-173.

de Morton, S.N., Wallace, M.W., Reed, C.P., Hewson, C., Redmond, P., Cross, E. and Moynihan, C., 2015. The significance of Tournaisian tectonism in the Dublin basin: implications for basin evolution and zinc-lead mineralization in the Irish Midlands. *Sedimentary Geology*, *330*, pp.32-46.

de Morton, S., Wallace, M.W., Reed, C., Hewson, C., Redmond, P., Cross, E. and Moynihan, C., 2015. The value of a combined approach: Innovative mineral exploration techniques in the Irish Zn-Pb orefield. *ASEG Extended Abstracts*, *2015*(1), pp.1-4.

Devuyst, F.X. and Lees, A., 2001. The initiation of Waulsortian buildups in Western Ireland. *Sedimentology*, *48*(5), pp.1121-1148.

Eaton, D.W., Milkereit, B. and Salisbury, M., 2003. Seismic methods for deep mineral exploration: Mature technologies adapted to new targets. *The leading edge*, *22*(6), pp.580-585.

Eaton, D.W., Adam, E., Milkereit, B., Salisbury, M., Roberts, B., White, D. and Wright, J., 2010. Enhancing base-metal exploration with seismic imaging. *Canadian Journal of Earth Sciences*, *47*(5), pp.741-760.

Eberli, G.P., Baechle, G.T., Anselmetti, F.S. and Incze, M.L., 2003. Factors controlling elastic properties in carbonate sediments and rocks. *The Leading Edge*, *22*(7), pp.654-660.

Elliott, H.A.L., Gernon, T.M., Roberts, S. and Hewson, C., 2015. Basaltic maar-diatreme volcanism in the Lower Carboniferous of the Limerick Basin (SW Ireland). *Bulletin of Volcanology*, *77*, pp.1-22.

Fusciardi, L.P., Guven, J.F., Stewart, D.R.A., Carboni, V., Walsh, J.J., Kelly, J.G., Andrew, C.J., Ashton, J.H., Boland, M.B., Earls, G. and Fusciardi, L., 2003. The geology and genesis of the Lisheen Zn-Pb deposit, Co. Tipperary, Ireland. *Europe's major base metal deposits*, pp.455-481.

Geological Survey of Ireland, 2022, Bedrock geology of Ireland map 1:100,000: Limerick Basin, Geological Survey of Ireland.

Gil, A., Malehmir, A., Buske, S., Alcalde, J., Ayarza, P., Martínez, Y., Lindskog, L., Spicer, B., Carbonell, R., Orlowsky, D. and Carriedo, J., 2021. Reflection seismic imaging to unravel subsurface geological structures of the Zinkgruvan mining area, central Sweden. *Ore Geology Reviews*, *137*, p.104306.

https://doi.org/10.5194/egusphere-2025-2512
Preprint. Discussion started: 10 June 2025

Gordon, P., Kelly, J. G. and van Lente, B., 2018. NI 43-101 Independent Report on the Zinc-Lead Exploration Project at Stonepark, County Limerick, Ireland. www.groupelevenresources.com/Projects/Stonepark.

Hitzman, M.W., 1999. Extensional faults that localize Irish syndiagenetic Zn-Pb deposits and their reactivation during Variscan compression. *Geological Society, London, Special Publications*, *155*(1), pp.233-245.

Hool, A., Helbig, C. and Wierink, G., 2024. Challenges and opportunities of the European critical raw materials act. *Mineral Economics*, *37*(3), pp.661-668.

Johnston, J.D., Coller, D., Millar, G. and Critchley, M.F., 1996. Basement structural controls on Carboniferous-hosted base metal mineral deposits in Ireland. *Geological Society, London, Special Publications*, *107*(1), pp.1-21.

Johnston, J.D., 1999. Regional fluid flow and the genesis of Irish Carboniferous base metal deposits. *Mineralium Deposita*, *34*, pp.571-598.

Kyne, R., Torremans, K., Güven, J., Doyle, R. and Walsh, J., 2019. 3-D modeling of the lisheen and silvermines deposits, County Tipperary, Ireland: insights into structural controls on the formation of Irish Zn-Pb deposits. *Economic Geology*, *114*(1), pp.93-116.

Lees, A.L.A.N., 1964. The structure and origin of the Waulsortian (Lower Carboniferous) "reefs" of west-central Eire. *Philosophical Transactions of the Royal Society of London. Series B, Biological Sciences*, *247*(740), pp.483-531.

Lees, A. and Miller, J., 1995. *Waulsortian banks* (Vol. 23, pp. 191-271). Oxford, UK: Blackwell Publ.

Liberty, L.M., Schmitt, D.R. and Shervais, J.W., 2015. Seismic imaging through the volcanic rocks of the Snake River Plain: Insights from Project Hotspot. *Geophysical Prospecting*, *63*(4-Hard Rock Seismic imaging), pp.919-936.

Malehmir, A., Durrheim, R., Bellefleur, G., Urosevic, M., Juhlin, C., White, D.J., Milkereit, B. and Campbell, G., 2012. Seismic methods in mineral exploration and mine planning: A general overview of past and present case histories and a look into the future. *Geophysics*, *77*(5), pp. WC173-WC190.

Malehmir, A., Manzi, M., Draganov, D., Weckmann, U. and Auken, E., 2020. Introduction to the special issue on "Cost-effective and innovative mineral exploration solutions". *Geophysical prospecting*, *68*(1), pp.3-6.

Manzi, M., Malehmir, A. and Durrheim, R., 2019. Giving the legacy seismic data the attention they deserve. *First Break*, *37*(8), pp.89-96.

McBride, J., Nelson, S.T., Mwakanyamale, K.E., Wolfe, E.E., Tingey, D.G. and Rey, K.A., 2021. Geophysical characterization of volcanic layering. *Journal of Applied Geophysics*, *195*, p.104494.

McCormack, T., O'Connell, Y., Daly, E., Gill, L.W., Henry, T. and Perriquet, M., 2017. Characterisation of karst hydrogeology in Western Ireland using geophysical and hydraulic modelling techniques. *Journal of Hydrology: Regional Studies*, *10*, pp.1-17.

Meere, P.A., 1995. The structural evolution of the western Irish Variscides: an example of obstacle tectonics? *Tectonophysics*, *246*(1-3), pp.97-112.

O'Connell, Y., Daly, E., Henry, T. and Brown, C., 2018. Terrestrial and marine electrical resistivity to identify groundwater pathways in coastal karst aquifers. *Near Surface Geophysics*, *16*(2), pp.164-175.

Paige, C.C. and Saunders, M.A., 1982. LSQR: An algorithm for sparse linear equations and sparse least squares. *ACM Transactions on Mathematical Software (TOMS)*, *8*(1), pp.43-71.

Planke, S., Alvestad, E. and Eldholm, O., 1999. Seismic characteristics of basaltic extrusive and intrusive rocks. *The Leading Edge*, *18*(3), pp.342-348.

Pu, Y., Liu, G., Wang, D., Huang, H. and Wang, P., 2021, September. Wave-equation traveltime and amplitude for Kirchhoff migration. In *First International Meeting for Applied Geoscience & Energy* (pp. 2684-2688). Society of Exploration Geophysicists.

Pujol, J., Fuller, B.N. and Smithson, S.B., 1989. Interpretation of a vertical seismic profile conducted in the Columbia Plateau

https://doi.org/10.5194/egusphere-2025-2512
Preprint. Discussion started: 10 June 2025

basalts. *Geophysics*, *54*(10), pp.1258-1266.

Sevastopulo, G.D. and Wyse Jackson, P.N., 2009. Carboniferous: Mississippian (Tournaisian and Viséan). *The geology of Ireland*, pp.215-268.

Singh, B. and Malinowski, M., 2023. Seismic imaging of mineral exploration targets: Evaluation of ray-vs. wave-equation-based pre-stack depth migrations for crooked 2d profiles. *Minerals*, *13*(2), p.264.

Sleeman, A.G., Pracht, M. and Claringbold, K., 1999. *Geology of the Shannon Estuary: A geological description of the Shannon Estuary region including parts of Clare, Limerick and Kerry to accompany the bedrock geology 1: 100,000 Scale Map Series, Sheet 17, Shannon Estuary*. Geological Survey of Ireland.

Slezak, P., Hitzman, M.W., van Acken, D., Dunlevy, E., Chew, D., Drakou, F. and Holdstock, M., 2023. Petrogenesis of the Limerick Igneous Suite: insights into the causes of post-eruptive alteration and the magmatic sources underlying the Iapetus Suture in SW Ireland. *Journal of the Geological Society*, *180*(2), pp.jgs 2022-039.

Slezak, P., Hnatyshin, D., Andrés, A., Dunlevy, E., Koch, H., Holdstock, M. and Hitzman, M.W., 2023. A review of the Limerick Igneous Suite: links to base-metal mineralization in the SW Irish Orefield. *Irish Association of Economic Geology. IAEG 50th Anniversary Volume*.

Somerville, I.D. and Jones, G.L., 1985. The Courceyan stratigraphy of the Pallaskenry Borehole, County Limerick, Ireland. *Geological Journal*, *20*(4), pp.377-400.

Somerville, I.D., Strogen, P. and Jones, G.L., 1992. Biostratigraphy of Dinantian limestones and associated volcanic rocks in the Limerick Syncline, Ireland. *Geological Journal*, *27*(3), pp.201-22 .

Somerville, I.D., Waters, C.N. and Collinson, J.D., 2011. South Central Ireland.

Strogen, P., 1983. *The geology of the volcanic rocks of southeast County Limerick* (Doctoral dissertation, University College Dublin).

Strogen, P., 1988. The Carboniferous lithostratigraphy of southeast County Limerick, Ireland, and the origin of the Shannon Trough. *Geological Journal*, *23*(2), pp.121-137.

Sullivan, E.C., Hardage, B.A., McGrail, B.P. and Davis, K.N., 2011. Breakthroughs in seismic and borehole characterization of basalt sequestration targets. *Energy Procedia*, *4*, pp.5615-5622.

Torremans, K., Kyne, R., Doyle, R., Güven, J.F. and Walsh, J.J., 2018. Controls on metal distributions at the Lisheen and Silvermines deposits: insights into fluid flow pathways in Irish-type Zn-Pb deposits. *Economic Geology*, *113*(7), pp.1455-1477.

Tryggvason, A., Rögnvaldsson, S.T. and Flóvenz, O.G., 2002. Three-dimensional imaging of the P-and S-wave velocity structure and earthquake locations beneath Southwest Iceland. *Geophysical Journal International*, *151*(3), pp.848-866.

Tryggvason, A. and Bergman, B., 2006. A traveltime reciprocity discrepancy in the Podvin & Lecomte time3d finite difference algorithm. *Geophysical Journal International*, *165*(2), pp.432-435.

Tyler, P.A., 1997. The geology and exploration potential of the Pallas Green project. *Unpublished internal report by McKillen, Tyler and Associates for Minco Ireland Limited*.

Vidal, O., Goffé, B. and Arndt, N., 2013. Metals for a low-carbon society. *Nature Geoscience*, *6*(11), pp.894-896.

Wilkinson, J.J., Hitzman, M.W., Archibald, S.M. and Piercey, S.J., 2015. The Irish Zn-Pb orefield: the view from 2014. *Current Perspectives on Zinc Deposits. Irish Association for Economic Geology, Dublin*, pp.59-72.

Ziolkowski, A., Hanssen, P., Gatliff, R., Jakubowicz, H., Dobson, A., Hampson, G., Li, X.Y. and Liu, E., 2003. Use of low frequencies for sub-basalt imaging. *Geophysical Prospecting*, *51*(3), pp.169-182.